Contents list available at CBIORE journal website

International Journal of Renewable Energy Development

Journal homepage: https://ijred.cbiore.id

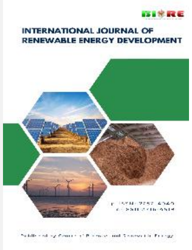

Research Article

Influence of profile geometry on the self-starting capability of an H-Darrieus turbine

Martínez-Oropeza Rogelio[a], J. C. García[a], Laura Castro Gómez[a], Itzel Vera-Wilimek[b], O. A. Jaramillo[c], José Omar Dávalos Ramírez[d]*

[a]*Center for Research in Engineering and Applied Sciences, Universidad Autónoma del Estado de Morelos, Morelos, México*

[b]*Center for Transdisciplinary Research in Psychology, Universidad Autónoma del Estado de Morelos, Morelos, México*

[c]*Institute of Renewable Energies, Universidad Nacional Autónoma de México, México*

[d]*Institute of Engineering and Technology, Universidad Autónoma de Ciudad Juárez, Chihuahua, México*

Abstract. To spread the use of Wind H-Darrieus turbines to electricity generation in urban or rural environments is necessary to improve some of its main drawbacks such as: aerodynamic efficiency, self-starting capability and torque fluctuations. The aims of this study are to enhance the aerodynamic efficiency and self-starting capability of an H-Darrieus turbine through wind tunnel tests combined using a 3D numerical study using Computational Fluid Dynamics (CFD). The NREL S815 profile and four modified versions were evaluated, including one with a 19.2% increase in thickness and three chord-to-diameter ratios: C/D=0.15, 0.20, and 0.225. These configurations were tested at wind speeds of 6 and 8 m/s. Static torque was measured experimentally, alongside numerical calculations of flow and pressure distribution. A significant correlation between chord length and turbine performance was observed. The C/D=0.20 profile exhibited increases of up to 50.27% and 58.88% in static torque at 6 and 8 m/s, respectively. The static torque coefficient increased from 0.0063 in the original profile to 0.0447 in the C/D=0.20 profile, directly contributing to the improvement of self-starting capability. Although the C/D=0.20 geometry showed improvements, the C/D=0.225 profile did not show additional performance gains, indicating that further increases in chord length do not improve turbine performance. The profile modified with a 19.2% increase in thickness ranked just below the C/D=0.2 profile, exhibiting torque increases of 41% and 25.22% at 6 and 8 m/s, respectively. These findings confirm that chord-to-diameter ratio adjustments play a critical role in boosting torque generation in vertical-axis wind turbines.

Keywords: H-Darrieus turbine, maximum thickness, NREL S815, profile chord, self-starting capability.

Received: 16th Feb 2025; Revised: 8th April 2025 ; Accepted: 5th May 2025; Available online: 17th May 2025

1. Introduction

Wind energy has proven to play a crucial role in addressing climate change and the global energy crisis, establishing itself over the last decade as one of the most cost-effective energy sources with high potential for electricity generation (Holstead *et al.*, 2017; He *et al.*, 2020; Maalouly *et al.*, 2022). In 2022, 78 GW of new capacity were added globally, bringing the total to 906 GW and projecting an increase of up to 1221 GW by 2027 (Hutchinson & Zhao, 2023). It is also expected to lead capacity growth alongside solar, until 2025, contributing to the reduction in fossil fuel use (Brauwer *et al.*, 2020; International Energy Agency, 2020). Wind turbines are generally classified into horizontal-axis (HAWTs) and vertical-axis (VAWTs) types (Hau, 2013; Kaya *et al.*, 2018; Tjiu *et al.*, 2015a). HAWTs are the most developed and widely used in large-scale wind farms (Li *et al.*, 2023; Tjiu *et al.*, 2015b), while VAWTs are better suited for urban environments due to their omnidirectional operation and their capacity to harness low-speed winds (Rezaeiha *et al.*, 2020; Toudarbari *et al.*, 2021).

VAWTs are classified according to how they harness the kinetic energy of the wind: turbines that operate primarily by drag forces, such as the Savonius, and those that operate by lift forces, such as the Darrieus turbine (Hand *et al.*, 2021; Tjiu *et al.*, 2015a). The latter has a variant known as H-Darrieus, which exhibits the highest efficiency levels among VAWTs (Wafula *et al.*, 2020). Despite the favorable characteristics of H-Darrieus turbines, they are also limited by low self-starting capability at certain angular positions (Huang *et al.*, 2023), and lower efficiency compared to HAWTs, due to rapid variations in the angle of attack experienced by each blade in every rotation cycle (Buchner *et al.*, 2015). To address these issues, several strategies have been proposed, including the incorporation of deflectors, slots, or variable pitch mechanisms (Jin *et al.*, 2018; Guo *et al.*, 2019; Zidane *et al.*, 2023; Benmoussa & Páscoa, 2023; Aziz *et al.*, 2025). However, these approaches are relatively complex and require the integration of additional components into the turbine. Alternatively, other studies have focused on modifying the geometric characteristics of turbine blades, including thickness, camber, and chord length, to enhance overall performance.

Hashem and Mohamed (Hashem & Mohamed, 2018) conducted a numerical study aimed at improving the efficiency

---

* Corresponding author
Email: jose.davalos@uacj.mx (J.O.D.Ramirez)

of an H-Darrieus turbine, evaluating 24 airfoils, both symmetrical and non-symmetrical, at different tip speed ratio (TSR) values, ranging from 2 to 7. They reported a maximum efficiency of 0.3463 for the S1046 profile. Mohamed *et al.* (Mohamed *et al.*, 2019), with the goal of improving both the efficiency and self-starting capability of the turbine, performed a numerical analysis in which they tested 25 airfoils and compared their performance with the NACA 0021 profile. They found that the LS (1)-0413 profile improved efficiency by 16% compared to the NACA 0021 profile, while also generating a higher static torque, indicating improved self-starting capability. Zhang et al (Zhang *et al.*, 2024) designed a straight-bladed vertical axis wind turbine without an intermediate support shaft to evaluate its performance under various configurations. They found that the best performance was achieved with a pitch angle of 10°, an installation radius of 160 mm, and a blade length of 600 mm. Isataev *et al.* (Isataev *et al.*, 2025) performed experimental and numerical studies to evaluate the performance of a Darrieus rotor with asymmetrical blades, with and without plates. They found that, at wind speeds between 3 and 6 m/s, the rotor with plates exhibited a torque increase of 18-22%, facilitating self-starting and improving operational stability.

Other studies have also investigated the self-starting and performance characteristics of H-Darrieus turbines, aiming to increase their static torque at angular positions where the extraction of kinetic energy is low. This limitation arises from the nature of rotary operation, which causes cyclic variations in the angle of attack of the blades with respect to the wind. Studies reveal that the asymmetric S815 profile has a higher static and dynamic torque coefficient compared to the EN0005 profile (Sengupta *et al.*, 2017; Sengupta *et al.*, 2019) and that increasing its thickness by 19.2% leads to a 14.96% improvement in efficiency at a wind speed of 8 m/s (Martinez *et al.*, 2021). Tong *et al.* (Tong *et al.*, 2023) used numerical simulations to investigate the effect of NACA 0018 airfoil chord length and rotor diameter on the aerodynamic performance of an H-Darrieus turbine. They identified the chord-to-diameter ratio, which is an important parameter in VAWT design. Xu *et al.* (Xu *et al.*, 2024) conducted numerical and experimental studies to evaluate the self-starting capability and the power output of turbines. They analyzed the effects of the static evaluation method on the dynamic start-up process. The investigation focused on the NACA 0018, NACA 2418, and NACA 4418 airfoils. They realized that at wind speeds of 5.5 and 6 m/s, the turbine generates positive torque between 0° and 60° azimuthal angles, while negative torque is observed between 60° and 120°, affecting the self-starting capability. However, this condition is overcome at 6 m/s, where no negative torque is observed.

Similarly, researchers have modified airfoils, mainly by suppressing one of the walls to form J-type blades, which has been shown to improve self-starting capability (Bel Laveda *et al.*, 2023; Celik *et al.*, 2023; Farzadi & Bazargan, 2023), as well as by adding tubercles to increase their power coefficient by reducing flow separation on the walls (Hassan *et al.*, 2023; Zulkefli *et al.*, 2024), and incorporating slots into the airfoils to improve the drag-to-lift ratio at different angles of attack during turbine rotation (Abdolahifar & Karimian, 2022; Akhter *et al.*, 2024; Bhavsar *et al.*, 2023).

The studies above show that the performance of H-Darrieus turbines depends on multiple factors, including solidity, TSR, angle of attack, and airfoil geometry. However, airfoil shape is one of the key factors influencing efficiency and self-starting capability. This study presents a wind tunnel investigation and a 3D numerical study using Computational Fluid Dynamics (CFD) to analyze the influence of turbine solidity and modification of the airfoil shape in a three-bladed H-Darrieus turbine, focusing on static torque generation throughout a full rotation. For this purpose, the S815 profile was selected as a reference due to its favorable results reported in previous studies (Martinez *et al.*, 2021; Sengupta *et al.*, 2019). To enhance its self-starting capability, four modifications were proposed: a 19.2% increase in maximum thickness and three chord length variations as a function of the rotor diameter, with C/D ratios of 0.15, 0.20, and 0.225, tested at wind speeds of 6 m/s and 8 m/s. Based on these tests, this work contributes by identifying the optimal C/D configuration that maximizes torque generation and improves self-starting capability, offering practical insight for the geometric design of H-Darrieus turbines.

2. Methodology

2.1 Experimental setup and instrumentation

The experiment was conducted in a low-speed wind tunnel with a length of 5 meters and a cross-sectional area of 0.5 meters by 0.5 meters. Figure 1a shows the dimensions of the wind tunnel and the layout of the test section. Tests were performed at wind speeds of 6 m/s and 8 m/s. To verify flow uniformity across the test section, wind speed measurements were taken along the horizontal midplane. Five measurement points (P1) were placed upstream of the test section, and five additional points (P2) were located downstream.

Velocity measurements were taken using a DWYER 471 digital hot-wire anemometer, which has a measurement range from 0 to 30 m/s and an uncertainty of ± 3% of full scale. The locations of the measurement points are shown in Figure 1b. Each main position, P1 and P2, comprises five measurement points distributed over the plane. From the data collected at these subpoints, velocity profiles were generated for both P1 and P2 at wind speeds of 6 m/s and 8 m/s, as illustrated in Figure 2.

2.2 H-Darrieus wind turbine

The turbine used in this study is a three-bladed H-Darrieus turbine with a diameter, D, of 0.29 m and a rotor height, H, of 0.29 m. Its dimensions were taken from the study conducted by Sengupta (Sengupta *et al.*, 2019). Figure 3 shows the dimensions and configuration of the experimental wind turbine model. The experimental array was assembled as follows: the rotation shaft and the turbine shaft were made of aluminum to minimize rotor

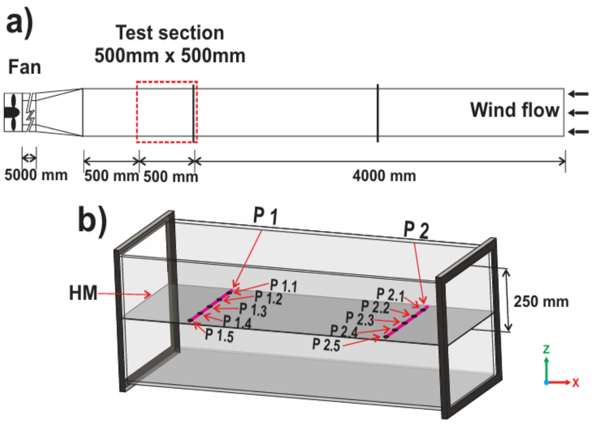

Fig 1. Wind tunnel description: a) 2D wind tunnel layout, b) measurement points P1 and P2 placed on the horizontal midplane

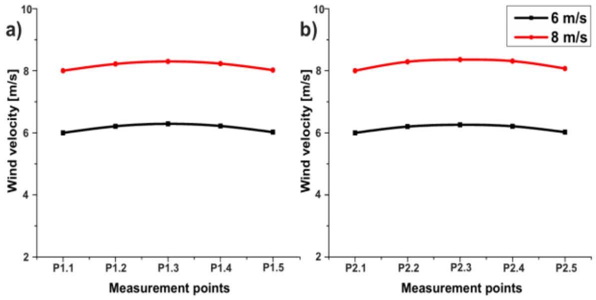

Fig 2. Velocity profiles measured for speeds of 6 m/s and 8 m/s at a) horizontal upstream points and b) horizontal downstream points.

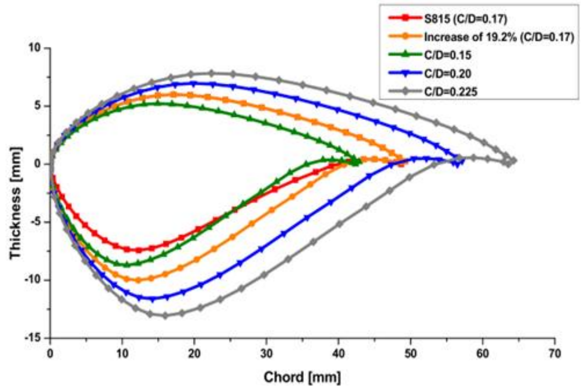

Fig 4. 2D coordinates of profiles examined in this study

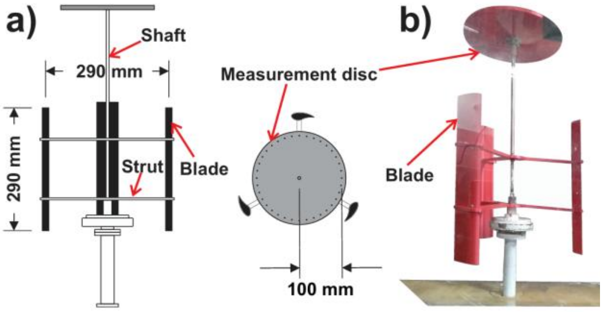

Fig 3. Dimensions and setup of the experimental array a) Wind turbine dimensions and b) photography of experimental array

Fig 5. Experimental setup for measurement disk and dynamometer for torque measurements

weight, while the blades, struts, and measuring disk were manufactured from polylactic acid with a fused deposition modeling technique. The evaluated profiles include the S815 profile and its four modifications, which consisted of increasing its maximum thickness by 19.2%, based on the results reported by Martínez *et al.* (Martínez *et al.*, 2021), and three variations in chord length, C, relative to the rotor diameter, D, with C/D values of 0.15, 0.20 and 0.225. The C/D ratios of 0.15, 0.20, and 0.225 were selected to evaluate configurations with smaller and larger chords relative to the original profile (S815), which has a chord length of 50 mm, corresponding to a C/D ratio of 0.1724. This range allows for a broader evaluation of the aerodynamic behavior as a function of the C/D ratio. Figure 4 shows the profiles evaluated in this study.

2.2 Static torque measurement

The static torque of the turbine for the different profiles was calculated using Equation (1) (Wong *et al.*, 2018; Zulkefli *et al.*, 2024), which is determined by the measured tangential force, $\boldsymbol{F}$, and the lever arm length, r, perpendicular to the axis of rotation. Using the obtained torque values, the static torque coefficient, $C\tau$, was calculated using Equation (2) (Wong *et al.*, 2018; Zulkefli *et al.*, 2024), where τ, ρ, V, A, R, represent static torque, air density, wind speed, swept area, and rotor radiius, respectively.

$$\tau = Fr \tag{1}$$

$$C_\tau = \frac{\tau}{0.5\rho V^2 AR} \tag{2}$$

The tangential force was measured using an IMADA DS2-11 digital dynamometer with an accuracy of ± (0.2% FS ± 1 LSD), anchored to a 3D-printed disc positioned at the end of the turbine shaft. Static torque was measured at different angular positions (every 10°), with 36 measurements per rotation using the 36 points evenly distributed on the printed disk. Once the dynamometer was anchored at each measurement point, the turbine was subjected to a constant wind speed, and the resulting force was recorded by the dynamometer. The setup for torque measurement is shown in Figure 5. The first measurement at 0° on the measuring disk was aligned with the center of mass of one blade, perpendicular to the wind flow. Subsequent measurements were performed in a counter-clock wise direction. Each test case was repeated three times, with a run time of 1 minute per test. The torque values reported in this paper represent the average of the three repeated tests.

2.2 Numerical simulation and CFD modeling

To analyze the flow behavior around the evaluated profiles in this study, steady-state simulations were conducted using CFD under identical wind conditions and azimuthal angles as those used in the experimental measurements. Each case study yielded results for static torque, velocity fields and pressure contours.

The semi-implicit method for pressure-linked equations (SIMPLE) algorithm was used to solve the Reynolds-averaged Navier-Stokes equations, given by Equations (3) and (4). Turbulence was modeled using the k-ε RNG turbulence model, with the transport equations for turbulent kinetic energy and energy dissipation rate given by Equations (5) and (6), respectively.

$$\frac{\partial \bar{u}_i}{\partial x_i} = 0 \tag{3}$$

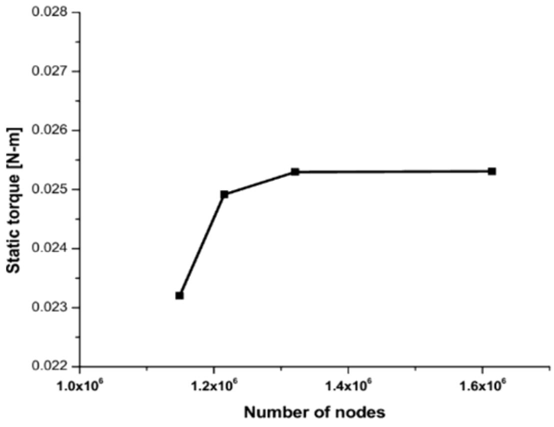

Fig 6 mesh convergence study

$$\frac{\partial \bar{u}_i}{\partial_t} + \bar{u}_j \frac{\partial \bar{u}_i}{\partial_{x_j}} = \frac{\partial \bar{p}}{\partial_{x_i}} + v \frac{\partial^2 \bar{u}_i}{\partial_{x_j} \partial_{x_j}} - \frac{\partial_{\tau_{ij}}}{\partial_{x_j}} \quad (4)$$

$$\frac{\partial}{\partial t}(\rho k) + \frac{\partial}{\partial x_i}(\rho k u_i) = \frac{\partial}{\partial x_j}\left[a_k \mu_{eff} \frac{\partial k}{\partial x_j}\right] + G_k + G_b - \rho\varepsilon - Y_M + S_k \quad (5)$$

$$\frac{\partial}{\partial t}(\rho \varepsilon) + \frac{\partial}{\partial x_i}(\rho \varepsilon u_i) = \frac{\partial}{\partial x_j}\left[a_k \mu_{eff} \frac{\partial \varepsilon}{\partial x_j}\right] + C_{1\varepsilon} \frac{\varepsilon}{k}(G_k + C_{3\varepsilon} G_b) - C_{2\varepsilon\rho} \frac{\epsilon^2}{k} - R_\epsilon + S_\varepsilon \quad (6)$$

The computational domain consists of two stationary volumes: a circular domain enclosing the turbine blades and a rectangular one representing the surrounding environment. The dimensions were determined based on the rotor diameter, with the outer domain extending 5 diameters upstream, 10 diameters downstream, and 5 diameters on each side of the turbine. The circular domain was set with a radius of 2 rotor diameters.

To ensure numerical accuracy while optimizing the computational cost of the CFD simulations, a mesh sensitivity study was conducted to verify that variations in mesh size had a minimal impact on the results. Four mesh configurations with varying levels of refinement were evaluated based on the computed static torque. These configurations corresponded to the following grid sizes: 1 149 064, 1 215 290, 1 321 123, and 1 614 285. The corresponding static torque values obtained for each configuration are shown in Fig. 6. The results show that, starting from mesh 3, the static torque tends to stabilize, with minimal variation as the mesh is further refined. Mesh 3 exhibited a relative error of less than 1% compared to the mesh 4, indicating that further refinement has a negligible effect on the calculated static torque. Based on these findings, mesh 3 was selected for all subsequent simulations due to its balance between computational efficiency and numerical accuracy. The resulting mesh is shown in Figure 7.

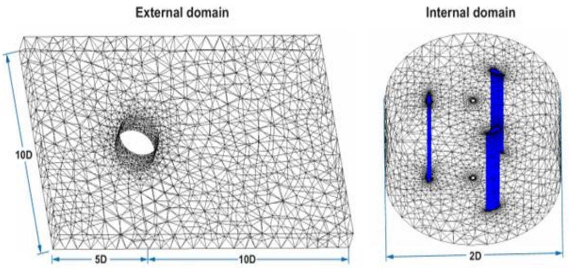

Fig 7. Meshes of internal and external domain

The boundary conditions for the numerical study were defined as follows: the velocity was specified in the x-direction with magnitudes of 6 and 8 m/s. A turbulence intensity of 5% was selected based on previous studies in low-speed wind tunnels, where this level was found to adequately represent the inlet and outlet flow conditions in experimental setups (Ghafoorian *et al.*, 2024; Zhao *et al.*, 2025; Ghafoorian *et al.*, 2025). The boundary condition at the walls and blades was no-slip, whereas at the interface between the external and internal domain was defined as a coupled interface.

The evaluation of the different angular positions of the turbine was carried out by manually rotating the interior domain in 10-degree increments, completing a full rotation for each case. A torque monitor was placed at the center of the rotation axis. To ensure convergence, the residuals were set to 1 × 10^{-6}. The mesh and numerical model were based on the study reported by Martinez (Martinez *et al.*, 2021).

3. Results and discussion

In this paper, experimental wind tunnel tests and numerical simulations were conducted at constant wind speeds of 6 m/s and 8 m/s. The objective was to investigate the effect of modifications to the S815 airfoil on the static torque generated by an H-Darrieus turbine throughout its rotation at different angular positions. Additionally, the relationship between the torque coefficient and the azimuthal angle was calculated and analyzed, focusing on the distribution of $\boldsymbol{C_\tau}$ at angular positions with low kinetic energy extraction rates. The objective was to enhance $\boldsymbol{C_\tau}$ at angular positions with low energy extraction, as this is critical for improving self-starting capability.

3.1 Effect of airfoil on turbine static torque

The aerodynamic performance of the H-Darrieus rotor is influenced by several factors as previously discussed. Airfoil geometry plays a critical role, as it alters the drag-to-lift ratio generated by the airflow interacting with the airfoil surfaces. These forces are also influenced by the turbine solidity and the wind speed. The airfoil profiles evaluated in this study induce changes in solidity due to variations in chord length, which modify the ratio between the turbine cross-sectional area, diameter, and the solid portion. The solidity values for each evaluated airfoil were calculated using Equation (7) (Miller *et al.*, 2021) and are presented in Table 1.

$$\boldsymbol{\sigma = \frac{NC}{D}} \quad (7)$$

Where $\boldsymbol{N}$ is the number of blades.

Figure 8 shows the evolution of the sum of the experimental static torques generated by the three blades when the turbine remains stationary at different azimuthal positions. These measurements were obtained under wind speeds of 6 m/s and 8 m/s while operating with different profiles. The oscillatory behavior of the static torque is observed throughout

Table 1
Turbine Solidity for the profiles examined in this study

Profile	Chord [mm]	Solidity
S815	50	0.517
Increase of 19.2%	50	0.517
$\boldsymbol{C/D}$=0.15	43.5	0.45
$\boldsymbol{C/D}$=0.20	58	0.6
$\boldsymbol{C/D}$=0.225	65.25	0.675

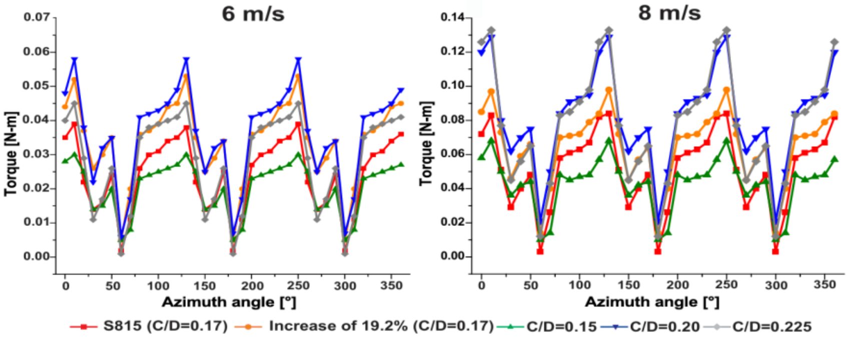

Fig 8 Experimental static torque for the different profiles at wind speeds of 6 and 8m/s

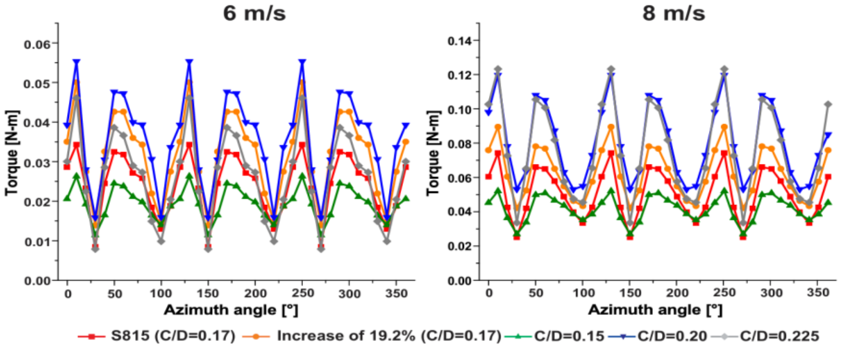

Fig 9. Computed static torque for the different profiles at wind speeds of 6 and 8m/s

a complete turbine rotation, with maximum values occurring at azimuthal positions of 10°, 130°, and 250°, which are considered favorable positions, and minimum values (unfavorable positions) at 60°, 180°, and 300°, where the torque is significantly reduced, indicating less efficient power generation during those phases.

The greatest difference in static torque generated at 6 m/s is observed at the peak points of the graph, where the original profile generates 0.039 N·m. This value is lower than that generated by the profile with a 19.2% increase in thickness, which reaches 0.052 N·m. Additionally, increasing the chord length leads to a progressive rise in peak torque from C/D=0.15 to C/D=0.20, which records the highest torque of 0.058 N·m. However, beyond this point, torque decreases, as seen in the C/D=0.225 case, which generates only 0.045 N·m. This performance drop at peak positions can be attributed to the increased surface area exposed to the flow, leading to a rise in drag relative to lift forces. As a result, drag dominance reduces the torque, especially at unfavorable angular positions where flow separation becomes more significant in excessively elongated chord profiles.

The evolution of the static torque for the turbine subjected to a wind speed of 8 m/s shows a similar pattern to that observed at 6 m/s. The maximum static torque values recorded for the S815 profile are lower than those for the profile with increased thickness, measuring 0.084 N·m and 0.098 N·m, respectively. Regarding the effect of chord length on static torque, the profile with C/D=0.225 exhibits the highest value, reaching 0.133 N·m, followed by the profile C/D=0.20. However, when examining the least favorable position, the C/D=0.20 profile achieves the highest value of all the profiles, reaching 0.021 N·m.

Figure 9 illustrates the evolution of the simulated static torque generated by the turbine at different azimuthal positions, using various airfoil profiles and wind speeds of 6 m/s and 8 m/s. Similar to the experimental data, the torque oscillation throughout the rotation reveals a pattern of three positions corresponding to maximum kinetic energy absorption and three corresponding to minimum absorption. While the azimuthal positions for the maximum points remain consistent, a 30° shift occurs in the least favorable positions. The least favorable azimuthal positions located at 30°, 150°, and 270°, are attributed to the presence of the struts supporting the profiles in the experimental model. These struts were excluded from the numerical simulation to reduce computational cost. Nevertheless, the torque behavior at both wind speeds shows strong agreement, with a maximum discrepancy of only 0.0021 N·m.

At a wind speed of 6 m/s, the torque generated at the favorable position is as follows: the profile with a C/D ratio of 0.15 exhibits the lowest static torque values, reaching 0.026 N·m. The S815 profile reaches 0.034 N·m, while the C/D=0.225 profile generates 0.045 N·m. The modified profile, with a 19.2% increase in thickness, generates a torque of 0.049 N·m, and the profile with C/D = 0.20 generates the highest value, reaching 0.055 N·m. In contrast, at unfavorable positions, both the S815 profile and the C/D = 0.22 profile generate the lowest torque values, 0.00835 N·m and 0.0078 N·m, respectively, while the C/D=0.20 profile registers the highest, reaching 0.015 N·m. At a wind speed of 8 m/s, a change in the torque distribution at the favorable position was observed, with the C/D=0.225 profile reaching the highest value, 0.123 N·m, surpassing the C/D=0.20 profile. However, at the least favorable position, the latter records the highest value (0.053 N·m). These results show strong agreement with the experimental findings.

3.2 Effect of solidity on the self-starting capability

A clear understanding of static torque distribution during turbine rotation is crucial for addressing the low self-starting

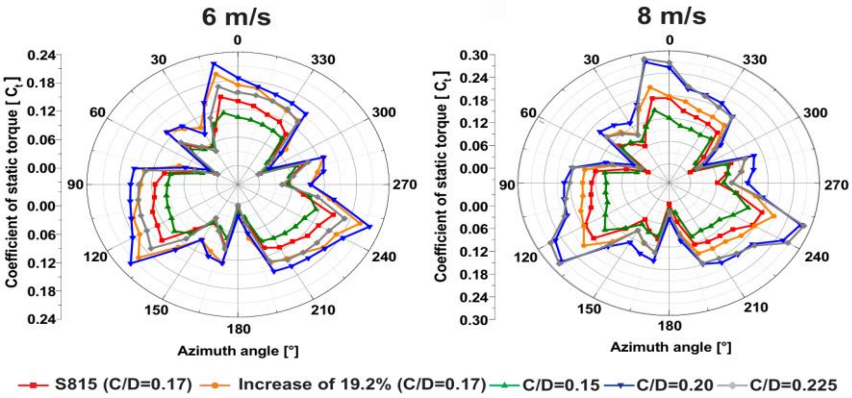

Fig 10. Instantaneous static torque coefficient of wind turbine during one rotation at wind speeds of 6 and 8m/s

capability, especially in unfavorable positions, where static torque values are low and may oppose rotation. In this section, the static torque coefficient is calculated using Equation (2) and analyzed based on the experimental data presented earlier. The analysis focuses primarily on unfavorable azimuthal positions, where kinetic energy extraction is limited. It also examines how turbine solidity affects the resulting static torque coefficient in such conditions.

Fig. 10 shows the polar distribution of the static torque coefficient at wind speeds of 6 m/s and 8 m/s, aiming to assess the influence of turbine solidity, affected by profile modifications, on self-starting capability. At 6 m/s, C_τ increases with a solidity of 0.6, which corresponds to the C/D=0.20 profile, where C_τ=0.0227. Beyond a solidity of 0.6, C_τ decreases again, with the C/D=0.225 profile showing the lowest coefficient. At 8 m/s, the S815 profile yields the lowest C_τ (0.0063), while the C/D=0.20 profile shows the highest (0.0447). These results demonstrate that at both wind speeds, the C/D=0.20 profile consistently produces the highest C_τ values under unfavorable conditions. At favorable positions, the maximum C_τ recorded was 0.219 at 6 m/s. This value exceeds that reported by Xu *et al.* (Xu *et al.*, 2024), who conducted tests on NACA 2018 and NACA 0018 airfoils with a turbine solidity of 0.8. They obtained a C_τ=0.034 at the same wind speed. Despite operating with lower solidity, the C/D=0.20 profile demonstrates superior self-starting capability.

3.3 Distribution of static pressure over the airfoil surface

The flow around the simulated turbine blades is analyzed through static pressure contours at azimuthal positions of 0°, 10°, 30°, and 60°. The first two correspond to the highest static torque values, whereas the latter correspond to the lowest. At these azimuthal positions, the original blade profile is compared with the modified profile with C/D=0.20, since the latter achieved the highest torque values.

Figures 11 and 12 illustrate the static pressure distributions on the turbine blades for the original profile (a) and the C/D=0.20 profile (b), under wind speeds of 6 and 8 m/s, respectively. The most significant differences are observed on blade 1 at azimuthal positions of 0° and 10°, where the C/D=0.20 profile exhibits a significant increase in static pressure on its upper surface compared to the original. This increase results in a larger force component aligned with the direction of turbine rotation, explaining the higher static torque observed. Similarly, at 30° and 60°, blades 1 and 2 exhibit the most notable differences in static pressure distribution. Specifically, for blade 1, the trailing edge of the upper surface contributes to generating a net force that favors rotation, while for blade 2, this effect occurs at the trailing edge of the lower surface. A comparison between the original profile and the C/D=0.20 profile at these positions reveals an increase in both static pressure and contact area. This explains the superior performance of the modified profile at these positions.

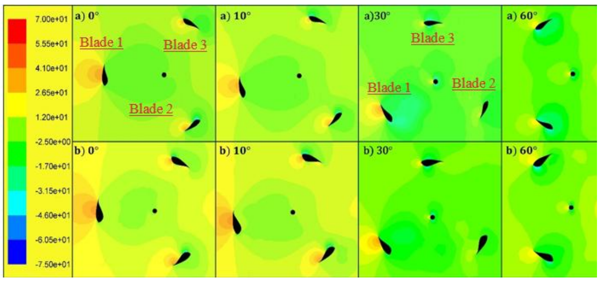

Fig 11 Contours of static pressure for different azimuthal angles at wind speed of 6m/s a) S815, b) C/D=0.20

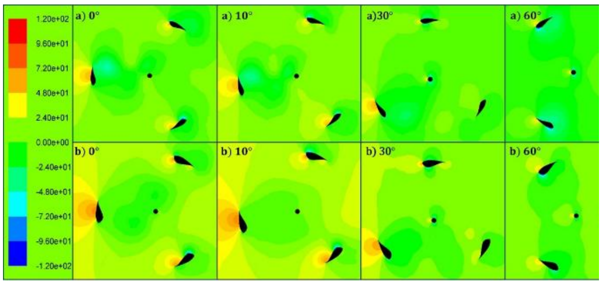

Fig 12 Contours of static pressure for different azimuthal angles at wind speed of 8m/s a) S815, b) C/D=0.20

Figures 13 and 14 show the streamline patterns at wind speeds of 6 and 8 m/s, respectively, under the same conditions used for the pressure contours. In Figure 13, at an azimuthal angle of 0°, the C/D=0.20 profile exhibits more pronounced vortex formation near the trailing edge, perpendicular to the incoming flow, compared to the S815 profile. This suggests more efficient torque generation. At 10° and 30°, the vortex structures also show greater definition and strength, with streamlines remaining attached longer, promoting lift generation and, consequently, increased torque. In contrast, the S815 profile exhibits early flow separation and a wider recirculation region. At 60°, both profiles experience flow

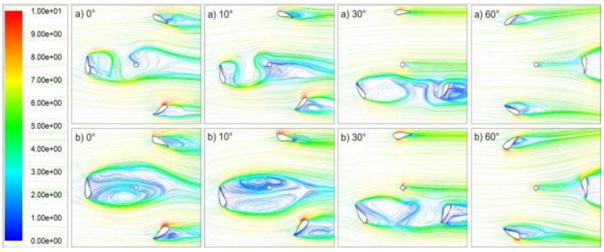

Fig 13 Streamlines for different azimuthal angles at wind speed of 6m/s a) S815, b) C/D=0.20

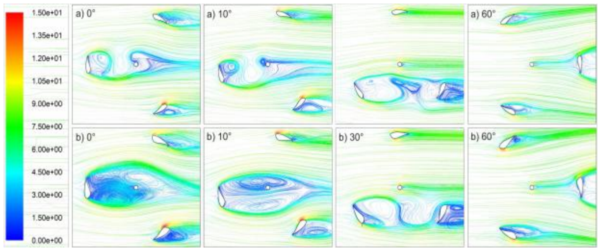

Fig 14 Streamlines for different azimuthal angles at wind speed of 8m/s a) S815, b) C/D=0.20

detachment; however, the transition is smoother for the modified profile, resulting in a more gradual shift into the next phase of the cycle. At 8 m/s, notable differences are observed in the flow interaction with each airfoil. At 0°, the $\boldsymbol{C/D}$=0.20 profile exhibits significantly stronger vortex formation on the surface perpendicular to the flow, compared to the S815 profile. At 10°, the formation of an attached vortex near the trailing edge is also enhanced, suggesting more efficient torque initiation through aerodynamic force generation. In contrast, the S815 profile displays a larger recirculation zone in the same region. At 30°, the S815 profile exhibits clear flow separation with an extended reverse flow region, which negatively impacts torque generation. In contrast, the C/D=0.20 profile manages separation more effectively, maintaining a compact and attached vortex that enhances the aerodynamic performance during this critical phase of rotation. Finally, at 60°, although both profiles exhibit low vortex generation, the modified design promotes a more stable reorganization of streamlines in the rear region, resulting in improved torque continuity during the descending phase of motion.

3.5 Average static torque in one rotation

The operation of the H-Darrieus rotor involves rotational motion, making it essential to evaluate the torque generated throughout a complete revolution using each profile. Measured results at each angular position are used to calculate the average torque per revolution for each profile under different wind speeds. These results are presented in Figure 15, which shows that at both wind speeds, the $\boldsymbol{C/D}$=0.20 profile exhibits the highest experimental and simulated static torque. Additionally, the modified profile with increased thickness outperforms the original profile at both wind speeds.

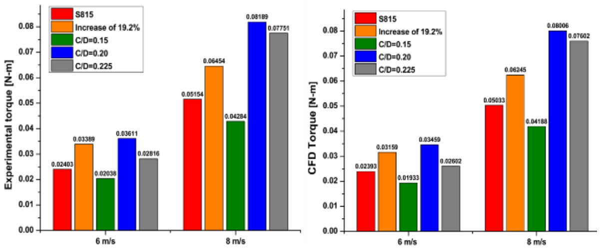

Fig 15 Experimental and CFD average static torque rotation at 6 and 8m/s

4. Conclusions

The objective of this work was to determine the influence of modifying the thickness and chord length of the S815 profile on the static torque generation throughout the rotational cycle of an H-Darrieus turbine, as well as their impact on self-starting capability. The experimental and simulated static torque values at different azimuthal positions show strong agreement, with differences of 6.37% at 6 m/s and 2.55% at 8 m/s, when using the C/D=0.20 profile as a reference. The profile with increased thickness generates higher experimental static torque than the S815 profile at all azimuthal positions for both wind speeds. The average increase in static torque was 41% at 6 m/s and 25.22% at 8 m/s for the modified profile. An increase in the chord length of the profiles directly affects the average C_τ of the turbine. The profile with a C/D ratio of 0.15 exhibits the lowest C_τ values at both wind speeds: 0.0771 at 6 m/s and 0.0911 at 8 m/s. These values increase with the C/D ratio, peaking at C/D= 0.20 with C_τ values of 0.1366 at 6 m/s and 0.1743 at 8 m/s. This results in an increase in static torque of 50.27% at 6 m/s and 58.88% at 8 m/s compared to the original profile. However, exceeding this C/D ratio results in a decrease in average torque. The evaluation of the self-starting capability focuses on the C_τ obtained at the unfavorable position, where a higher value indicates improved self-starting capability. The results show an upward trend at 6 m/s for each profile in the following order: C/D=0.225, S815, C/D=0.15, with a 19.2% increase, followed by C/D=0.20. At 8 m/s, the order is as follows: S815, C/D=0.15, C/D=0.225, 19.2% increase, followed by C/D=0.20. This confirms that the profile with the highest self-starting capability is the one with a ratio of C/D=0.20, with C_τ values of 0.0227 and 0.0447 at 6 m/s and 8 m/s, respectively. The static torques generated by the flow interaction with the turbine blades in unfavorable positions are primarily influenced by blades 1 and 2, which generate greater static pressure, creating in a force vector that favors rotation. Consequently, the C/D = 0.20 profile exhibits the highest static torque values at both wind speeds. These findings suggest that the optimal C/D=0.20 profile, which demonstrates the highest self-starting capability and static torque generation, could be applied to real-world turbine designs, particularly in small-scale and urban environments. Incorporating modifications, such as adjusting the chord length and solidity, can significantly enhance the efficiency and operational stability of H-Darrieus turbines, especially under low-wind conditions. The results also suggest the potential integration of additional features, such as slots, to further improve self-starting capability and overall turbine performance.

Acknowledgments

The main author would like to thank the National Council for Humanities, Science, and Technology (CONAHCyT) for the economic support for his graduate studies (Grant No. 745525) which contributed to the development of this work.

Author Contributions: R.M: Conceptualization, methodology, J.G.; supervision, R.M and IV: CFD calculations, RM and LC: experimental measurements, JD: data curation, O.J.: review and editing. All authors discussed the results and wrote the manuscripts. All authors have read and agreed to the published version of the manuscript.

Conflicts of Interest: The authors declare no conflict of interest.

References

Abdolahifar, A., & Karimian, S. M. H. (2022). A comprehensive three-dimensional study on Darrieus vertical axis wind turbine with slotted blade to reduce flow separation. *Energy*, *248*, 123632. https://doi.org/10.1016/j.energy.2022.123632

Akhter, M. Z., Jawahar, H. K., Omar, F. K., & Elnajjar, E. (2024). Performance characterization of a slotted wind turbine airfoil featuring passive blowing. *Energy Reports*, 11(November 2023), 720–735. https://doi.org/10.1016/j.egyr.2023.12.027

Aziz, M., Khalifa, M. A., Abdelrahman, M. A., Elshimy, H., & Elsayed A. M. (2025). Multi-slotted airfoil design for enhanced aerodynamic performance and economic efficiency. *Scientific Reports*, 15, 4290. https://doi.org/10.1038/s41598-025-87000-z

Bel Laveda, O., Roche, M. A., Phadtare, M., Sauge, L., Xavier, K. J., Bhat, G., Saxena, D., Saini, J. S., & Verdin, P. G. (2023). Numerical Investigation of Aerodynamic Performance and Structural Analysis of a 3D J-Shaped Based Small-Scale Vertical Axis Wind Turbine. *Energies*, 16(20). https://doi.org/10.3390/en16207024

Benmoussa, A., & Páscoa, J. C. (2023). Enhancement of a cycloidal self-pitch vertical axis wind turbine performance through DBD plasma actuators at low tip speed ratio. *International Journal of Thermofluids*, 17, 100258. https://doi.org/10.1016/j.ijft.2022.100258

Bhavsar, H., Roy, S., & Niyas, H. (2023). Aerodynamic performance enhancement of the DU99W405 airfoil for horizontal axis wind turbines using slotted airfoil configuration. *Energy*, 263(PA), 125666. https://doi.org/10.1016/j.energy.2022.125666

Brauwer, C. P. De, Ellis, G., Wade, R., & Volkmer, S. A. (2020). REN21 *Global Status Report* 2020 (Issue August).

Buchner, A., Lohry, M. W., Martinelli, L., Soria, J., & Smits, A. J. (2015). Dynamic stall in vertical axis wind turbines : Comparing experiments and computations. *Journal of Wind Engineering and Industrial Aerodynamics*, 146, 163–171. https://doi.org/10.1016/j.jweia.2015.09.001

Celik, Y., Ingham, D., Ma, L., & Pourkashanian, M. (2023). Novel hybrid blade design and its impact on the overall and self-starting performance of a three-dimensional H-type Darrieus wind turbine. *Journal of Fluids and Structures*, 119, 103876. https://doi.org/10.1016/j.jfluidstructs.2023.103876

Farzadi, R., & Bazargan, M. (2023). 3D numerical simulation of the Darrieus vertical axis wind turbine with J-type and straight blades under various operating conditions including self-starting mode. *Energy*, 278(PB), 128040. https://doi.org/10.1016/j.energy.2023.128040

Ghafoorian, F., Enayati, E., Mirmotahari, S. R., &Wan, H. (2024). Self-starting improvement and performance enhancement in Darrieus VAWTs using auxiliary baldes and deflectors. *Machines*, 12, 806. https://doi.org/10.3390/machines12110806

Ghafoorian, F., Mirmotaharai, S.R., Eydizadeh, M., & Mehrpooya, M. (2025). A systematic investigation on the hybrid Darrieus-Savonius vertical axis wind turbine aerodynamic performance and self starting capability improvement by installing a curtain. *Next Energy*, 6, 100203. https://doi.org/10.1016/j.nxener.2024.100203

Guo, Y., Li, X., Sun, L., Gao, Y., Gao, Z., & Chen, L. (2019). Aerodynamic analysis of a step adjustment method for blade pitch of a VAWT. *Journal of Wind Engineering & Industrial Aerodynamics*, 188(February), 90–101. https://doi.org/10.1016/j.jweia.2019.02.023

Hand, B., Kelly, G., & Cashman, A. (2021). Aerodynamic design and performance parameters of a lift-type vertical axis wind turbine: A comprehensive review. *Renewable and Sustainable Energy Reviews*, 139(January). https://doi.org/10.1016/j.rser.2020.110699

Hashem, I., & Mohamed, M. H. (2018). Aerodynamic performance enhancements of H-rotor Darrieus wind turbine. *Energy*, 142, 531–545. https://doi.org/10.1016/j.energy.2017.10.036

Hassan, S. S. ul, Javaid, M. T., Rauf, U., Nasir, S., Shahzad, A., & Salamat, S. (2023). Systematic investigation of power enhancement of Vertical Axis Wind Turbines using bio-inspired leading edge tubercles. *Energy*, 270(October 2022), 126978. https://doi.org/10.1016/j.energy.2023.126978

Hau, E. (2013). Wind Turbines: Fundamentals, Technologies, Application, Economics. *Springer Science & Business Media*. https://doi.org/10.4324/9780203103289-9

He, J., Jin, X., Xie, S., Cao, L., Wang, Y., Lin, Y., & Wang, N. (2020). CFD modeling of varying complexity for aerodynamic analysis of H-vertical axis wind turbines. *Renewable Energy*, 145, 2658–2670. https://doi.org/10.1016/j.renene.2019.07.132

Holstead, K. L., Galán-Díaz, C., & Sutherland, L. A. (2017). Discourses of on-farm wind energy generation in the UK farming press. *Journal of Environmental Policy and Planning*, 19(4), 391–407. https://doi.org/10.1080/1523908X.2016.1224157

Huang, H., Li, J., & Li, G. (2023). Improving the self-starting and operating characteristics of vertical axis wind turbine by changing center distance in part of blades. *Journal of Building Engineering*, 68(January), 105974. https://doi.org/10.1016/j.jobe.2023.105974

Hutchinson, M., & Zhao, F. (2023). *Global Wind Report* | GWEC. Global Wind Energy Council.

International Energy Agency. (2020). *Analysis and Forecast to 2025,* Executive Summary.

Isataev, M., Manatbayeb, R., Seydulla, Z., Kalassov, N., Yershina, A., & Baizhuma, Zhandos. (2025). Experimental and computational study of the aerodynamic characteristics of a Darrieus rotor with assymetrical blades to increase turbine efficiency under low wind velocity conditions. *Applied system Innovation*, 8, 49. https://doi.org/10.3390/asi8020049

Jin, X., Wang, Y., Ju, W., He, J., & Xie, S. (2018). Investigation into parameter influence of upstream deflector on vertical axis wind turbines output power via three-dimensional CFD simulation. Renewable *Energy*, 115, 41–53. https://doi.org/10.1016/j.renene.2017.08.012

Kaya, M. N., Kose, F., Ingham, D., Ma, L., & Pourkashanian, M. (2018). Aerodynamic performance of a horizontal axis wind turbine with forward and backward swept blades. *Journal of Wind Engineering and Industrial Aerodynamics*, 176(December 2017), 166–173. https://doi.org/10.1016/j.jweia.2018.03.023

Li, X., Zhou, S., & Zhao, Y. (2023). Onshore and offshore wind power generation forecasting using a novel flexible time-varying fractional nonlinear grey model. *Energy Conversion and Management*, 297, 117695. https://doi.org/10.1016/j.enconman.2023.117695

Maalouly, M., Souaiby, M., ElCheikh, A., Issa, J. S., & Elkhoury, M. (2022). Transient analysis of H-type Vertical Axis Wind Turbines using CFD. *Energy Reports*, 8, 4570–4588. https://doi.org/10.1016/j.egyr.2022.03.136

Martinez, R., Urquiza, G., Castro, L., & C., G. J. (2021). Shape effect of thickness of the NREL S815 profile on the performance of the H-rotor Darrieus turbine. *Journal of Renewable and Sustainable Energy*, 13(1). https://doi.org/10.1063/5.0015083

Miller, M. A., Duvvuri, S., & Hultmark, M. (2021). Solidity effects on the performance of vertical-axis wind turbines. *Flow*, 1, E9. https://doi.org/10.1017/flo.2021.9

Mohamed, M. H., Dessoky, A., & Alqurashi, F. (2019). Blade shape effect on the behavior of the H-rotor Darrieus wind turbine: Performance investigation and force analysis. *Energy*, 179, 1217-1234. https://doi.org/10.1016/j.energy.2019.05.069

Rezaeiha, A., Montazeri, H., & Blocken, B. (2020). A framework for preliminary large-scale urban wind energy potential assessment : Roof-mounted wind turbines. *Energy Conversion and Management*, 211(March), 112770. https://doi.org/10.1016/j.enconman.2020.112770

Sengupta, A. R., Biswas, A., & Gupta, R. (2017). The aerodynamics of high solidity unsymmetrical and symmetrical blade H-Darrieus rotors in low wind speed conditions. *Journal of Renewable and Sustainable Energy*, 9(4), 1–11. https://doi.org/10.1063/1.4999965

Sengupta, A. R., Biswas, A., & Gupta, R. (2019). Comparison of low wind speed aerodynamics of unsymmetrical blade H-Darrieus rotors-blade camber and curvature signatures for performance improvement. *Renewable Energy*, 139, 1412–1427. https://doi.org/10.1016/j.renene.2019.03.054

Tjiu, W., Marnoto, T., Mat, S., Ruslan, M. H., & Sopian, K. (2015a). Darrieus vertical axis wind turbine for power generation I: Assessment of Darrieus VAWT configurations. *Renewable Energy*, 75, 50–67. https://doi.org/10.1016/j.renene.2014.09.038

Tjiu, W., Marnoto, T., Mat, S., Ruslan, M. H., & Sopian, K. (2015b). Darrieus vertical axis wind turbine for power generation II: Challenges in HAWT and the opportunity of multi-megawatt Darrieus VAWT development. *Renewable Energy*, 75, 560–571. https://doi.org/10.1016/j.renene.2014.10.039

Tong, G., Li, Y., Tagawa, K., & Feng, F. (2023). Effects of blade airfoil chord length and rotor diameter on aerodynamic performance of straight-bladed vertical axis wind turbines by numerical simulation. *Energy*, 265(November 2022), 126325. https://doi.org/10.1016/j.energy.2022.126325

Toudarbari, S., Maghrebi, M. J., & Hashemzadeh, A. (2021). Evaluation of Darrieus wind turbine for different highway settings using CFD simulation. *Sustainable Energy Technologies and Assessments*, 45. https://doi.org/10.1016/j.seta.2021.101077

Wafula, D., Otieno, C., & Ngugi, J. (2020). An experimental investigation into performance characteristics of H-shaped and Savonius-type VAWT rotors. *Scientific African*, 10, 2468–2276. https://doi.org/10.1016/j.sciaf.2020.e00603

Wong, K. H., Chong, W. T., Sukiman, N. L., Shiah, Y. C., Poh, S. C., Sopian, K., & Wang, W. C. (2018). Experimental and simulation investigation into the effects of a flat plate deflector on vertical axis wind turbine. *Energy Conversion and Management*, 160 (October 2017), 109–125. https://doi.org/10.1016/j.enconman.2018.01.029

Xu, Z., Dong, X., Li, K., Zhou, Q., Zhao, Y., (2024). Study of the self starting performance of a vertical-axis wind turbine. *Journal of Applied Fluid Mechanics*, 17, 1261-1276. https://doi.org/10.47176/jafm.17.6.2295

Zhang, H., Hu, Y., & Wang, W. (2024). Wind tunnel experimental study on the aerodynamic characteristics of straight-bladed vertical axis wind turbine. *International Journal of Sustainable Energy*, 43, 2305035. https://doi.org/10.1080/14786451.2024.2305035

Zhao, Z., Chen, K., Wang, Q., Su, T., & Hu, H. (2025) Parameter optimization of a H-type three-blade contra-rotating vertical-axis wind turbine at low tip-speed ratio. *Journal of Applied Fluid Mechanics*, 18 (6), 1470-1482. https://doi.org/10.47176/jafm.18.6.3189

Zidane, I. F., Ali, H. M., Swadener, G., Eldrainy, Y. A., & Shehata, A. I. (2023). Effect of upstream deflector utilization on H-Darrieus wind turbine performance: An optimization study. *Alexandria Engineering Journal*, 63, 175–189. https://doi.org/10.1016/j.aej.2022.07.052

Zulkefli, N. F., Nurdin, M. A., & Nur, N. M. (2024). Performance Analysis of H-Rotor Darrieus Wind Turbine with Whale Tubercles Leading Edge Blades. *Journal of Aeronautics, Astronautics and Aviation*, 56(1), 365–373. https://doi.org/10.6125/JoAAA.202403_56(1S).25